

# Characterization of Freestanding AlN Single Crystals Grown Through a Novel Approach Using the PVT Method

Wang Zhihao, Wang Qikun, He Guangdong, Lei Dan, Huang Jiali, Wu Liang

State Key Laboratory of Advanced Special Steel, Shanghai University, Shanghai 200444, China

**Abstract:** A novel approach to grow freestanding AlN single crystals spontaneously using the physical vapor transport (PVT) method was presented. Dozens of single crystals can be obtained on the surface of a pre-sintered AlN powder source in a single growth run using this approach. The largest AlN single crystal grown at 2373~2523 K for 100 h is 7 mm×8 mm×12 mm, and the typical diameter is 5~7 mm. The surface morphologies of the as-grown crystals were investigated by scanning electron microscopy, whereas the structural quality of the crystals was characterized by Raman spectroscopy and high-resolution X-ray diffraction. Raman spectroscopy exhibits an  $E_2$  (high) full width at half maximum (FWHM) of 5.7  $\text{cm}^{-1}$ , whereas the high-resolution X-ray diffraction rocking curve shows a FWHM of 93.6 arc-second for the symmetric reflection. The average etch pit density revealed by preferential chemical etching is  $7.5 \times 10^4 \text{ cm}^{-2}$ , and the major impurities determined by evolved gas analysis and glow discharge mass spectrometry are carbon of 28  $\mu\text{g}\cdot\text{g}^{-1}$  and oxygen of 120  $\mu\text{g}\cdot\text{g}^{-1}$ . The proposed novel approach provides a new means of obtaining high-quality AlN single crystals, which can be cut into wafers and are ideal as seeds for subsequent homoepitaxial AlN growth. Using these small seeds, crack-free bulk AlN single crystal/wafers that have excellent deep UV transparency and that are up to 60 mm in diameter were successfully prepared.

**Key words:** AlN substrates; physical vapor transport; surface morphology; structural quality

Aluminum nitride (AlN) is a promising substrate material for the epitaxial growth of wide-bandgap nitride semiconductors<sup>[1]</sup>. AlN is suitable for high-frequency, high-power, high-temperature, and deep UV optoelectronic devices because of its wide bandgap, high breakdown field, and high thermal conductivity<sup>[2]</sup>. Currently, the lack of large high-quality AlN substrates restricts the fabrication of III-nitride semiconductor devices<sup>[3]</sup>. The physical vapor transport (PVT) growth method has shown to be the only reasonable technique to produce high-quality bulk AlN crystals<sup>[4-6]</sup>. Homoepitaxial seeding on SiC and homoepitaxial seeding on native AlN are typical techniques employed to grow large-sized AlN crystals using the PVT method. At present, industrial-sized AlN crystals can be fabricated by SiC seeding with a dislocation density (DD) of  $10^6 \sim 10^8 \text{ cm}^{-2}$ <sup>[7-9]</sup>. However, lower DD values ( $\text{DD} < 10^6 \text{ cm}^{-2}$ ) are needed for deep UV devices. These low dislocation densities on AlN substrates can only be obtained

by homoepitaxial seeding on native AlN.

Because AlN does not occur naturally as a mineral, two main approaches are used to obtain AlN seeds using the PVT method: (1) by selecting grains from freely nucleated AlN polycrystals on planar crucible lids or in a crucible with a conical end, and (2) by obtaining grains from self-nucleated AlN crystals on a perforated diaphragm. In the past decades, considerable effort has been devoted to growing inch-sized AlN single crystals using the PVT method, and considerable advances have been made using homoepitaxial seeding growth based on obtaining high-quality AlN seeds<sup>[10]</sup>. However, additional reported methods of preparing high-quality AlN seeds with a decent size are limited.

In this study, a novel approach to grow freestanding AlN crystals spontaneously using the PVT method was presented. Dozens of AlN single crystals were harvested from the surface of a pre-sintered AlN powder source after sublimation growth.

Received date: October 25, 2019

Foundation item: National Natural Science Foundation of China (61874071)

Corresponding author: Wu Liang, Ph. D., Professor, State Key Laboratory of Advanced Special Steel, Shanghai University, Shanghai 200444, P. R. China, Tel: 0086-21-66138042, E-mail: lwu@shu.edu.cn

Copyright © 2020, Northwest Institute for Nonferrous Metal Research. Published by Science Press. All rights reserved.

The surface morphologies of the as-grown crystals were investigated by scanning electron microscopy (SEM), whereas the structural quality of the crystals was characterized by Raman spectroscopy and high-resolution X-ray diffraction (HRXRD). Evolved gas analysis (EGA) and glow discharge mass spectrometry (GDMS) were employed to determine major impurities, and the preferential chemical etching in molten eutectic KOH/NaOH alloy was adopted to evaluate the etch pit density (EPD) in the as-grown crystals.

## 1 Experiment

Crystal growth experiments were conducted using our in-house resistively heated sublimation reactor loaded with a 76-mm-diameter tungsten crucible, as shown in Fig.1a. Prior to each sublimation growth experiment, the AlN powder source was sintered in a tungsten crucible to remove the carbon and oxygen impurities and to obtain a dense starting material for subsequent sublimation growth. The typical growth conditions are as follows. A high-purity nitrogen atmosphere (99.999%) was maintained at 30~70 kPa, and the temperature of the pre-sintered AlN powder source was maintained at 2373~2523 K. The charge of the pre-sintered AlN powder source was 350~450 g, and the distance between the pre-sintered AlN powder source and the crucible lid was 40~60 mm. In addition, the evaluated temperature gradient between the AlN source and crucible lid was 1.2~2.0 K/mm as calculated by FAMAG software. The simulation result with a temperature control point of 2373 K at the center of the

crucible bottom is shown in Fig.1b. More details related to the hot zone and heat transfer simulations were provided in Ref.[11].

Dozens of Al- and N-polar freestanding crystals were grown simultaneously on the same surface of the pre-sintered AlN powder source using the proposed novel approach. The Al-polar crystals were light yellow with excellent transparency, whereas the N-polar crystals were brown without transparency. The as-grown facets of most crystals showed mirror-like surfaces. Some crystals even had as-grown c-plane facets with mixed Al- and N-polar polarities. The largest AlN single crystal had dimensions of 7 mm×8 mm×12 mm with a typical hexagonal prism shape formed by mirror-like m-plane  $\{10\bar{1}0\}$  facets, as presented in Fig.2a, with a typical diameter of 5~7 mm.

## 2 Results and Discussion

### 2.1 Growth rate analysis

The estimated growth rate is typically calculated using the following equation<sup>[12,13]</sup>:

$$V_g = c \frac{\exp(A-B/T)}{T^{1.2} P^{1.5}} \cdot \frac{\Delta T}{\delta} \quad (1)$$

where  $c$ ,  $A$ , and  $B$  are constant and calculated to be 407.54, 27.055, and 75788, respectively.  $\Delta T$  and  $\delta$  represent the temperature difference and distance between the source surface and growth interface, respectively. Experimentally, the axial and radial growth rates are between 100~150  $\mu\text{m}/\text{h}$  and 50~60  $\mu\text{m}/\text{h}$  under the aforementioned growth conditions. However, compared to this proposed novel approach, both the axial and radial growth rates are higher than the rates evaluated by Eq.(1). Because Eq.(1) was derived from a one-dimensional model, the vapor transport distance  $\delta$  was estimated as the distance between the source surface and deposition interface (crucible lid). Nevertheless, this estimate is not valid for a novel approach when growing crystals on a pre-sintered powder surface. The growth rate and size differences can be explained as follows. First, the AlN crystal growth rate is proportional to the temperature where the nucleation occurs, whereas in this study the AlN crystal growth temperature at the top surface of the pre-sintered AlN powder source was 20~50 K higher than that of the tungsten crucible lid in this growth chamber. Second, the AlN crystal growth rate is inversely proportional to  $\delta$ , whereas growth on the pre-sintered AlN powder source has a much smaller  $\delta$  when compared to growth on the crucible lid. Finally, the local supersaturation simulated by this in-house code (not shown) on the surface of the pre-sintered AlN powder source is much lower as compared to that on the crucible lid. Therefore, stress-free crystals with high structural perfection, appreciable size, and low nucleation density can be grown under these close-to-equilibrium conditions<sup>[14,15]</sup>.

### 2.2 Surface morphologies of as-grown crystals

To investigate the growth behavior and surface morpho-

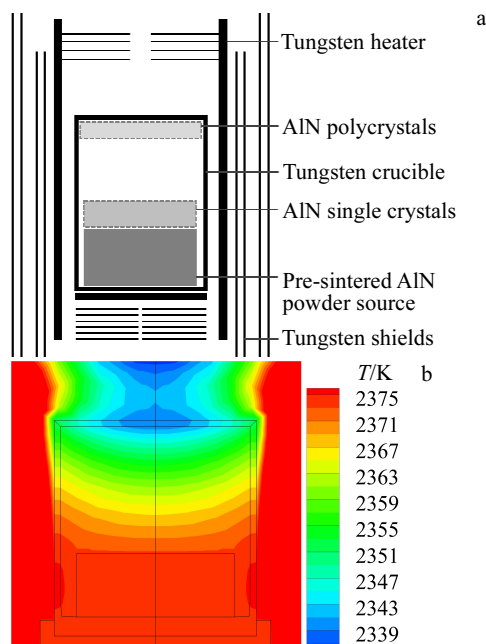


Fig.1 Schematic of the AlN crystal growth chamber (a); temperature distribution in the AlN crystal growth chamber (b)

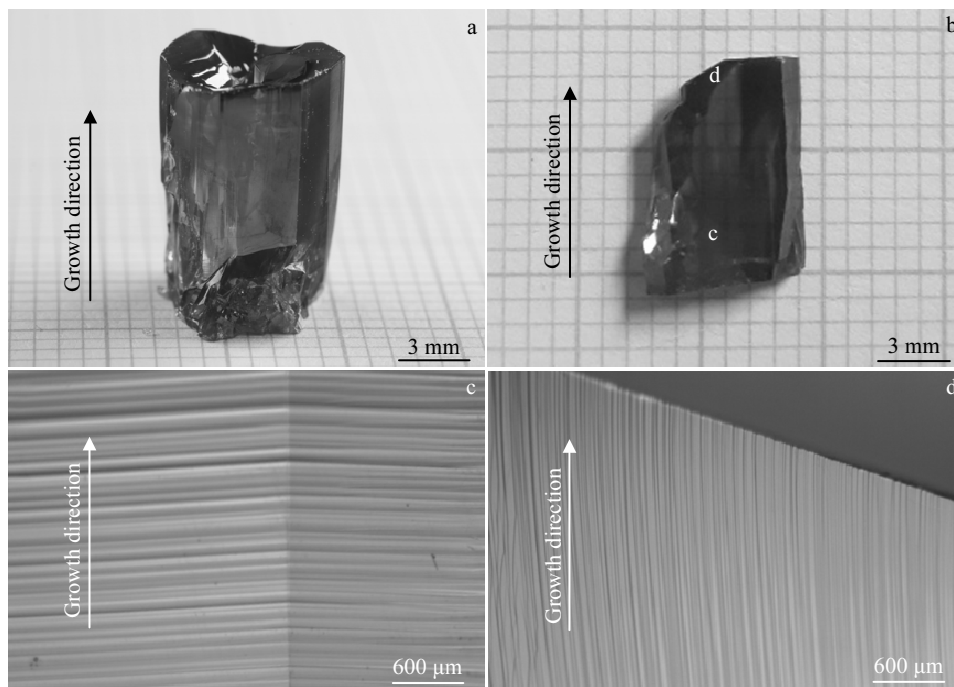


Fig.2 Spontaneously nucleated freestanding AlN single crystal grown on the pre-sintered AlN powder source at 2373~2523 K for 100 h (a); m-plane wafer cut from a spontaneously nucleated freestanding crystal (b); surface morphology of point c (c) and point d (d) in Fig.2b

logies, m-plane wafers were cut from one typical freestanding crystal, as shown in Fig.2b. Surface morphologies at different locations on these wafers were examined using an optical microscope. Fig.2c shows that the  $c$ -axis [0001] is the main growth orientation in the early growth stage. The growth terraces are 80~120  $\mu\text{m}$  in width and perpendicular to the growth direction. However, the  $m$ -axis [10 $\bar{1}$ 0] or the  $a$ -axis [11 $\bar{2}$ 0] finally became the dominant growth orientation within the next several millimeters, as shown in Fig.2d. The growth terraces parallel to the growth direction first form on the edges of the m-plane, and then coalesces gradually with further growth. As a result, the growth along the  $c$ -axis slows and finally stops. This outcome may explain the limitation of continuous crystal growth in this experiment.

The as-grown and sliced  $c$ -plane facets of the obtained crystals were investigated by selective wet-etching in a molten eutectic NaOH-KOH alloy. Because of the inhomogeneous nature of the defects, the selective wet-etching produced hexagonal etch pits on the Al-polar surface or hillocks on the N-polar surface under appropriate etching conditions. Because the Al-polar surface showed higher stability, the etching rate of the Al-polar surface was significantly lower than that of the N-polar surface<sup>[16-18]</sup>.

Fig.3a presents the etch pits after 180 s of etching at 633 K for an as-grown Al-polar surface. The estimated average EPD is approximately  $7.5 \times 10^4 \text{ cm}^{-2}$ . Hexagonal pyramids could be observed after 60 s of etching at 453 K for an as-grown

N-polar surface, as illustrated in Fig.3b. Small pyramids of several microns in diameter and covering most of the surface area are observed, whereas some bigger pyramids of 20~30  $\mu\text{m}$  in diameter form in lines or on the border of the top surface. The pyramids all have a 6- or 12-fold symmetrical structure formed by rhombohedral sidewall facets. A special  $c$ -plane surface with mixed Al- and N-polar polarities is etched for 30 s at 513 K, as demonstrated in Fig.3c. A terrace forms after etching due to the different etching rates of the Al- and N-polar regions, and the boundary between the two regions is parallel to the  $m$ -axis. This result indicates that a polarity inversion occurs during crystal growth. Shigetoh et al.<sup>[19]</sup> reported that the initial oxygen impurity incorporation was the origin of the polarity inversion during the PVT growth. However, this conclusion does not explain the growth results obtained by the proposed novel approach, as all the freestanding crystals on the surface of the pre-sintered AlN powder source were nucleated and grown simultaneously under identical growth conditions, including the concentration of oxygen impurity. The origin of the polarity inversion must be further investigated.

### 2.3 Structural quality of as-grown crystals

HRXRD and Raman spectroscopy were used to investigate the structural quality of the as-grown AlN single crystals. The HRXRD rocking curve reveals a FWHM of 93.6 arc-second for symmetric reflection on a  $c$ -plane surface of an Al-polar AlN crystal, as illustrated in Fig.4. This value is much lower

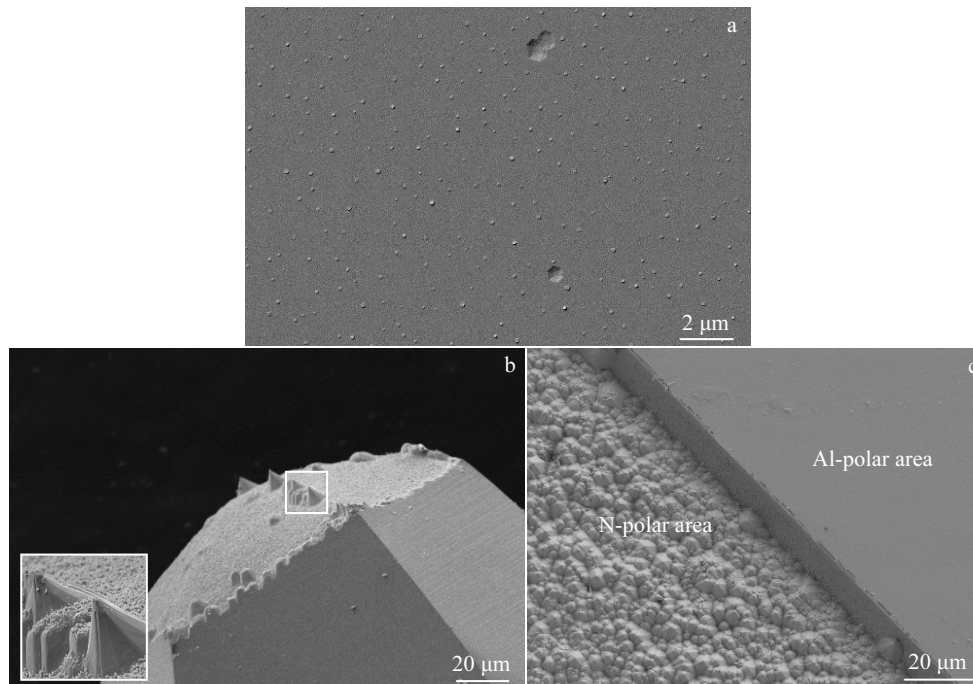


Fig.3 Al-polar (0001) facet after 180 s of etching at 633 K (a); N-polar ( $000\bar{1}$ ) facet after 60 s of etching at 453 K (b); c-plane surface with mixed Al-polar/N-polar facet after 30 s of etching at 513 K (c) in molten eutectic KOH/NaOH alloy

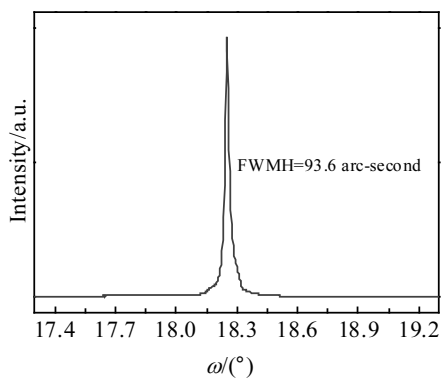


Fig.4 X-ray rocking curve of AlN single crystal grown on the pre-sintered AlN powder source

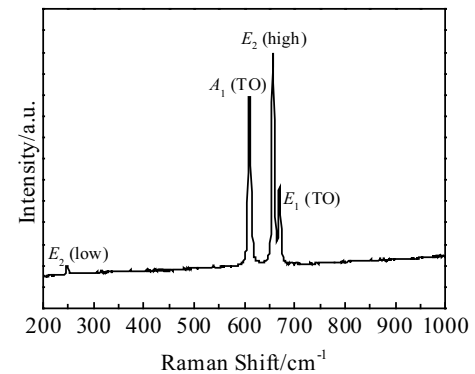


Fig.5 Raman spectrum of AlN single crystal grown on the pre-sintered AlN powder source

than that of crystals grown by heteroepitaxy<sup>[20]</sup> but is still higher than that of crystals grown by homoepitaxy<sup>[21]</sup>. Raman spectroscopy analysis with 532 nm laser excitation was performed on an m-plane surface of an Al-polar AlN crystal to evaluate the structural quality of the wafers and the residual stress inside the wafers. Only  $A_1$  (TO),  $E_2$  (high),  $E_2$  (low), and  $E_1$  (TO) modes could be observed. As shown in Fig.5 and Table 1, the Raman spectrum exhibits an  $E_2$  (high) peak with a very small Raman shift, for which the FWHM is  $5.7 \text{ cm}^{-1}$ . Compared with the results from Ref. [22], the as-grown single

**Table 1 Raman spectrum parameters of as-grown AlN corresponding to Fig.5**

Observed phonon mode	Raman shift/ $\text{cm}^{-1}$ (As-grown crystal)	Raman shift/ $\text{cm}^{-1}$ (Crystal in Ref.[22])	FWHM/ $\text{cm}^{-1}$ (As-grown crystal)
$E_2$ (low)	248	248	6.5
$A_1$ (TO)	610	610	5.9
$E_2$ (high)	657	656	5.7
$E_1$ (TO)	670	669	6.3

**Table 2 Major impurities measured by EGA and GDMS ( $\mu\text{g}\cdot\text{g}^{-1}$ )**

Element	C	O	W	Si	Fe	Na	B
Powder source	<600	<12000	-	70	20	-	-
As-grown crystal	28.0	120	<5.0	2.5	<0.50	<0.1	<0.05
Crystal in Ref.[22]	<100	<86	7.9	2.5	0.15	7.3	-

crystals are nearly stress-free.

It is common knowledge that the major impurities in bulk AlN crystals are oxygen, carbon, and silicon, which result in the generation of point defects and additional optical transitions<sup>[23]</sup>. Therefore, EGA and GDMS measurements were performed to determine the major impurities in the initial powder source and bulk crystals, as presented Table 2. It should be noted that all other trace impurities not listed in Table 2 are low and below the GDMS measurement limits. It could be seen that carbon and oxygen are reduced to quite low levels after the sintering process and crystal growth (carbon and oxygen are 28 and 120  $\mu\text{g}\cdot\text{g}^{-1}$ , respectively), although they are still the dominant impurities in the as-grown crystals.

Using the small AlN seeds prepared by the free-standing growth method, crack-free bulk AlN single crystals/wafers with diameter up to 60 mm and with excellent deep UV transparency were successfully prepared<sup>[24]</sup>. However, the proposed novel approach is still in its infancy and needs further investigation, such as the growth behavior and polarity inversion mechanism, in order to obtain even larger-size and higher-quality AlN seeds for subsequent AlN PVT homoe-pitaxial process, which is key to grow inch-size high-quality AlN crystals for UV LED applications.

### 3 Conclusions

1) A novel approach to grow freestanding AlN single crystals spontaneously using the physical vapor transport method is presented. Using this approach, dozens of single crystals can be obtained on the surface of a pre-sintered AlN powder source in a single growth run.

2) The HRXRD rocking curve reveals an FWHM of 93.6 arc-second, which is much lower than that of crystals grown by heteroepitaxy. Raman spectra exhibit an  $E_2$  (high) peak with a very small Raman shift, for which the FWHM is 5.7  $\text{cm}^{-1}$ , indicating that there is almost no residual stress in these crystals. The estimated average EPD is approximately  $7.5 \times 10^4 \text{ cm}^{-2}$ , showing a lower DD value as well.

3) Carbon and oxygen are the dominant impurities in the as-grown crystals, but their values are reduced to quite low levels after the sintering process and crystal growth. Carbon and oxygen are 28 and 120  $\mu\text{g}\cdot\text{g}^{-1}$ , respectively.

4) The largest AlN single crystal growth at 2373~2523 K

for 100 h is 7 mm×8 mm×12 mm, and the typical diameter is 5~7 mm.

### References

- Hirayama H, Enomoto Y, Kinoshita A et al. *Applied Physics Letters*[J], 2002, 80(1): 37
- Ambacher O. *Journal of Physics D: Applied Physics*[J], 1998, 31(20): 2653
- Wang W J, Zuo S B, Bao H Q et al. *Crystal Research and Technology*[J], 2011, 46(5): 455
- Noveski V, Schlessler R, Raghothamachar B et al. *Journal of Crystal Growth*[J], 2005, 279(1): 13
- Epelbaum B M, Bickermann M, Nagata S et al. *Journal of Crystal Growth*[J], 2007, 305(2): 317
- Sumathi R. *Physica Status Solidi (c)*[J], 2014, 11(3): 545
- Kim M, Fujita T, Fukahori S et al. *Applied Physics Express*[J], 2011, 4(9): 92 102
- Shatalov M, Sun W H, Lunev A et al. *Applied Physics Express*[J], 2012, 5(8): 82 101
- Dong P, Yan J C, Wang J X et al. *Applied Physics Letters*[J], 2013, 102(24): 241 113
- Hartmann C, Dittmar A, Wollweber J et al. *Semiconductor Science and Technology*[J], 2014, 29(8): 84 002
- Wang Z H, Deng X L, Cao K et al. *Journal of Crystal Growth*[J], 2017, 474: 76
- Wu B, Zhang H. *International Journal of Heat and Mass Transfer*[J], 2004, 47(14): 2989
- Liu L H, Edgar J H. *Journal of Crystal Growth*[J], 2000, 220(3): 243
- Hartmann C, Wollweber J, Dittmar A et al. *Japanese Journal of Applied Physics*[J], 2013, 52(8S): 8JA6
- Darakchieva V, Paskov P P, Paskova T et al. *Applied Physics Letters*[J], 2002, 80(13): 2302
- Bickermann M, Schmidt S, Epelbaum B M et al. *Journal of Crystal Growth*[J], 2007, 300(2): 299
- Zhuang D, Edgar J H, Strojek B et al. *Journal of Crystal Growth*[J], 2004, 262(1): 89
- Zhuang D, Edgar J H. *Materials Science and Engineering R: Reports*[J], 2005, 48(1): 1
- Shigetoh K, Horibuchi K, Nakamura D. *Journal of Crystal Growth*[J], 2017, 478: 33
- Sumathi R R, Gille P. *Japanese Journal of Applied Physics*[J], 2013, 52(8S): 8JA02
- Lu P, Collazo R, Dalmau R F et al. *Journal of Crystal Growth*[J], 2009, 312(1): 58
- Bickermann M, Epelbaum B M, Winnacker A. *Physica Status Solidi (c)*[J], 2003, 7: 1993
- Hartmann C, Wollweber J, Sintonen S et al. *Cryst Eng Comm*[J], 2016, 18(19): 3488
- Wang Q K, Lei D, He G D et al. *Physica Status Solidi (a)*[J], 2019, 216(16): 1 900 118

## 以物理气相传输法自支撑生长氮化铝单晶的表征

王智昊, 王琦琨, 贺广东, 雷丹, 黄嘉丽, 吴亮

(上海大学 省部共建高品质特殊钢冶金与制备国家重点实验室, 上海 200444)

**摘要:** 提出了用物理气相传输法自支撑生长氮化铝单晶的新方法, 此方法可以在氮化铝烧结体表面一次性获得大量生长的氮化铝单晶。在 2373~2523 K 的温度条件下经过 100 h 生长的氮化铝单晶, 其最大尺寸为 7 mm×8 mm×12 mm, 典型直径为 5~7 mm。这些原生晶体的表面形貌及结晶质量分别通过扫描电子显微镜、拉曼光谱和高分辨 X 射线衍射进行表征分析。拉曼光谱  $E_2$  峰位的半高全宽为  $5.7 \text{ cm}^{-1}$ , 高分辨 X 射线衍射得到的对称摇摆曲线的半高全宽为 93.6 弧度秒。经过选择性化学腐蚀后的晶体, 其表面的平均腐蚀坑密度为  $7.5 \times 10^4 \text{ cm}^{-2}$ 。逸出气体分析和辉光放电质谱分析结果表明, 碳和氧为晶体内部的主要杂质元素, 含量分别为 28 和 120  $\mu\text{g/g}$ 。此方法为高质量氮化铝单晶的获取提供了一个新的途径, 这些单晶可以被切成晶片作为后续氮化铝同质外延生长的优良籽晶。使用这些小的籽晶, 成功制备出了直径高达 60 mm 的氮化铝单晶体/晶圆, 并具有良好的深紫外光透过性。

**关键词:** 氮化铝衬底; 物理气相传输; 表面形貌; 结构质量

---

作者简介: 王智昊, 男, 1990 年生, 博士, 上海大学材料科学与工程学院, 上海 200444, 电话: 021-66138042, E-mail: wangzhihao021@yeah.net